Open Access Journal
Journal of Power Technologies 93 (3) (2013) 149–153
journal homepage:papers.itc.pw.edu.pl

Dynamic Modeling in a Switched Reluctance Motor SRM using Finite Elements

Abderrazak Guettaf[a], Foued Chabane[*,c], Ali Arif[a], Said Benramache[b]

[a]*Electrical Engineering Laboratory, Faculty of Technology*
University of Biskra 07000, Algeria
[b]*Material Sciences Department, Faculty of Science*
University of Biskra 07000, Algeria
[c]*Mechanics Department, Faculty of Sciences & Technology*
University of Biskra 07000, Algeria

Abstract

This paper study the dynamic modeling of a three phase 6/4 switched reluctance motor (SRM). We have studied electromagnetic field models using the finite element method (FEM) for calculation flux linkage and static torque. Modeling determined a nonlinear of dynamic model, the SRM model was then tested in a Matlab/Simulink environment, using nonlinear 2D look-up tables created from its calculated flux linkage and static torque data. Simulation studies were performed for hysteresis and voltage control strategies.

Keywords: Switched reluctance motor, Static converter, Control, Finite element, Analysis

1. Introduction

Switched reluctance motors (SRMs) perform well, featuring reliability and a high torque/weight ratio [1–3]. The high torque/weight ratio derives from the large reluctance torque for salient poles of both stator and rotor [4–6]. Switched reluctance has a good application foreground in some special fields, such as electrical traction for electric locomotives in coal mines, robust structures, high power density, fault-tolerant capability, high efficiency over a wide speed range, suitable for operating in unfriendly situations, and a high torque/weight ratio etc. [7–11]. However, the behavior of the SRM is strongly affected by the nonlinear magnetization characteristics of the constructed magnetic materials. Therefore, the magnetization behaviors of the SRMs are particularly important parameters in terms of predicting performance and studying advanced control strategies [12, 13].

The main disadvantage of SMRs the pulsed or non-uniform nature of the torque production, which leads to torque ripples and may contribute to acoustic noise. These torque ripples are sensitive to the size, mechanical construction and precision of the switching angles. Torque ripples are also correlated with current ripples (in the DC supply) which in turn may cause significant AC line harmonics. There are many strategies and methods to reduce or eliminate torque ripples in this type of machine. Essentially, there are two main approaches to reduce oscillations: the first consists of improving the magnetic design of the machine, while the second is based on electronic control. Torque is developed by the tendency for

*Corresponding author
Email addresses: fouedmeca@hotmail.fr (Foued Chabane*), benramache.said@gmail.com (Said Benramache)

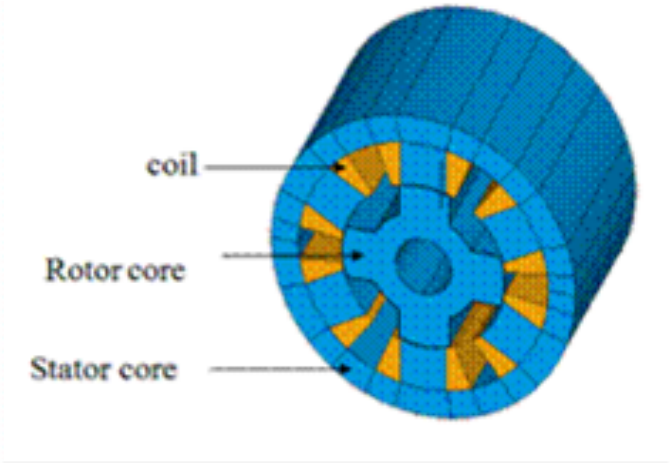

Figure 1: Reluctance machine variable

the magnetic circuit to adopt a configuration of minimum reluctance or to maximize the inductance of the excited coils. Since SRM uses reluctance torque which comes from the change of reluctance of the magnetic circuit, accurate estimation of the inductance depending on the rotor position is very important.

In this paper, we present a method for calculating the dynamic characteristics of SRM. (FEA) was used to estimate the non-linear inductance. Then, using the estimated inductance, a dynamic analysis model was constructed using FEMM. The method for determining the dynamic characteristics and simulated results are presented in section 2. The SRM model was then tested in a Matlab/ Simulink environment, using nonlinear 2D look-up tables created from its calculated flux linkage and static torque data. Simulation studies were performed for hysteresis and voltage control strategies.

2. Structure characterization of SRM

The structure of 8/6 SRM is presented in Fig. 1, which shows the schematic diagram of a six-stator pole, four-rotor pole; the stator and rotor laminations are assumed to be made of M-19 Non-Grain-Oriented Silicon Steels. Stator windings are chosen to have a vacuum relative permeability of one. The stator winding is concentrated and the rotor has no winding or brushes; see Figs. 2a and 2b for the construction details of this machine. The rotor has segments which constitute flux guides that serve to bend

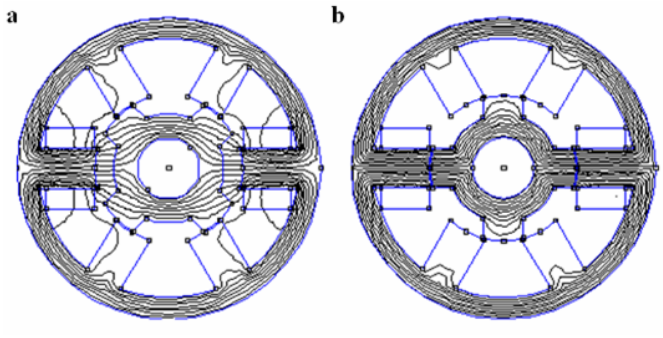

Figure 2: Flux distribution of SRM

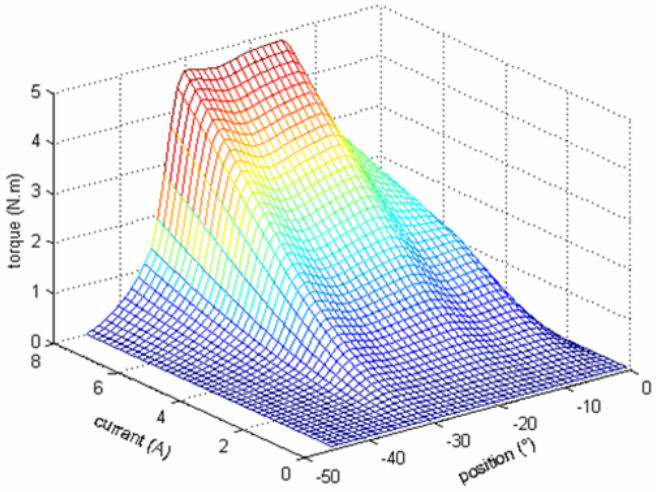

Figure 3: 3D plots of typical torque characteristics

the flux produced by the current flowing in the coil windings in the stator slots around the slot and back towards the periphery of the rotor.

Two typical flux distributions of the SRM are shown in Figs. 2a and 2b, which also show that the rotor axis is completely aligned and unaligned with the stator poles respectively. Since the flux distribution plots display the details of the magnetic field over the entire cross-section, locating local saturation and magnetic force distribution by inspection of flux plots becomes straight formation regarding the SRM terminal characteristics.

The torque-position-current curves are the most important characteristics of SRMs. Fig. 3 is used to show the correlation of the current and rotor angle of the torque: the so-called magnetization curves. The torque diagram plots instantaneous phase torque against the full range of rotor displacement in various phase currents. In order to identify the symmetry

of the phases, the curves of flux linkage and instantaneous inductance are measured for rotor positions varying from -45° to 0°.

3. Command Dynamic Characteristics of a SRM

The instantaneous voltage applied to the rolling up of a phase of SRM is given by:

$$V_i = Ri_i + \frac{d\psi_i(\theta, i_i)}{dt}, \quad i = \{1, 2, 3\} \tag{1}$$

Due to the double salience construction of the SRM and the magnetic saturation effects, the flux linked in an SRM phase varies as a function of rotor position θ and the phase current, Eq. (1) can be expanded as:

$$V = Ri + \frac{d\psi}{di}\frac{di}{dt} + \frac{d\psi}{d\theta}\frac{d\theta}{dt} \quad ou \tag{2}$$

$\frac{\partial\Psi}{\partial i}$: is defined as $L(\theta, I)$, the instantaneous inductance. $\frac{\partial\Psi}{\partial\theta}\frac{\partial\theta}{\partial t}$: is the instantaneous back electromotive force (EMF)

Whatever the vectors ψ and I are, the function of co-energy, they verify the following inequality:

$$\overline{W}(I, \theta) + W(\Psi, \theta) \geq \Psi^t I \tag{3}$$

The partial derivative of the energy function in relation to the rotor position gives the machine torque:

$$C_e(\Psi_1, \Psi_2, \Psi_3, \theta) = \frac{\partial W}{\partial\theta}(\Psi_1, \Psi_2, \Psi_3, \theta) \tag{4}$$

When one energizes one phase, the torque appears so that the rotor evolves in the direction where the inductance increases. Therefore, the torque will be in the direction of the nearest aligned position.

And the motor total torque by:

$$C_e = \sum_{i=1}^{3} C_{e_i}(i_i, \theta_i) \tag{5}$$

The mechanical equations are:

$$J\frac{d\omega}{dt} = C_e - C_r - f\omega \tag{6}$$

and

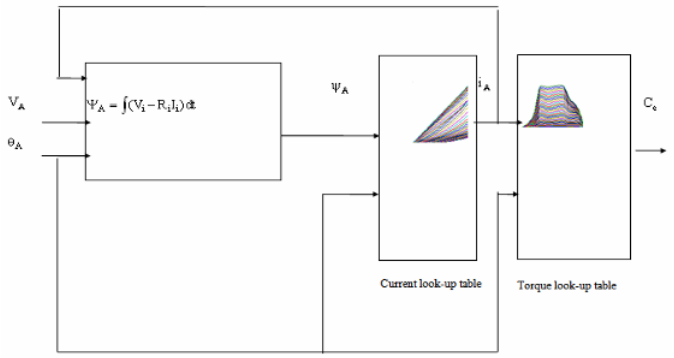

Figure 4: One phase nonlinear dynamic model of SRM

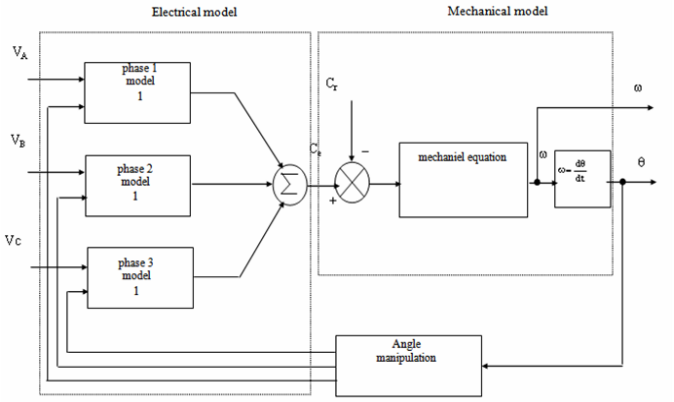

Figure 5: Dynamic model of the 3-phase SRM

$$\frac{d\theta}{dt} = \omega \tag{7}$$

The key to achieving a good simulation of an SRM is to use a methodology that permits the nonlinearity of its magnetic characteristic while minimizing the simulation time, the procedure that we used with Matlab-Simulink consisted in avoiding all partial derivatives, as they would be a source of error. The technique was to utilize a look-up table.

The proposed SRM dynamic model utilizes the look-up table of calculated characteristics (from the previous subsection) to estimate phase current and phase torque when the input voltage and the rotor position are known. Fig. 4. shows the schematic diagram of the one-phase dynamic model. It can be noticed that flux linkage as input to the current look-up table, can be found from the solution of:

$$\psi_{i=} \int (v_i - R_i i_i)\, dt \tag{8}$$

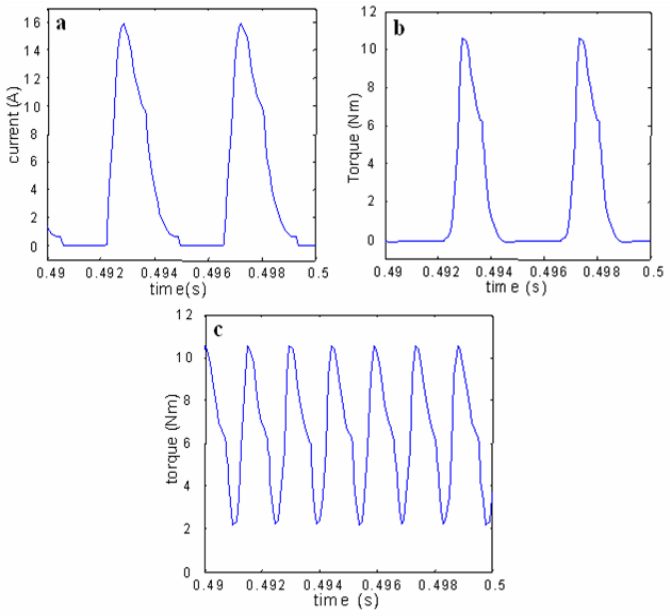

Figure 6: (a) Current in phase, (b) Torque in phase and (c) Total torque

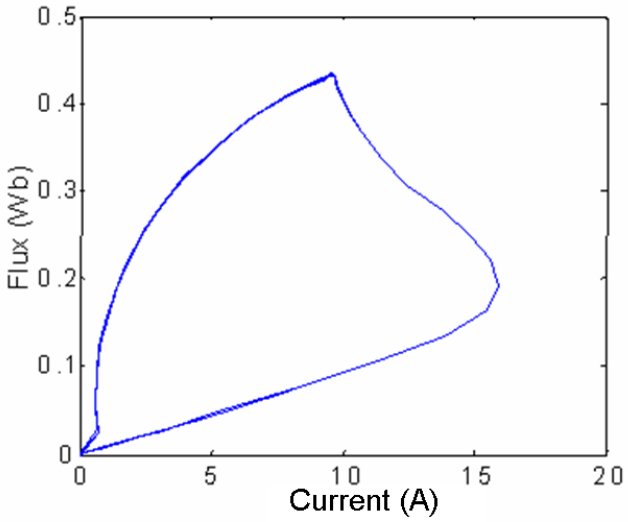

Figure 7: Co-energy

When all three models are integrated and the mechanical subsystem is included, a complete nonlinear dynamic model of the SRM can be formed (see Fig. 5).

3.1. Strategy—voltage source

Fig. 6 shows a second set of simulation resultants using $\theta_{on} = 0°$ and $\theta_{off} = 30°$, and with the motor functioning without load applied. One can see in Fig. 6a that the θ_{off} angle value is now sufficient to avoid the current starting to grow when the aligned position is reached. As expected, one can see in Fig. 6b that the phase current produces a very small negative torque. However, the total torque is always positive, as shown in Fig. 6c.

It is interesting to note the flux linkage current trajectory of the phase winding as shown. The operating points for one-phase current impulse is plotted while the rotor is rotating as compared to Fig. 7. The area circled out by the trajectory equals the co-energy variant for the cycle. The average torque production of SRM then can be computed from the co-energy variation of the phase winding with respect to the incremental rotor angle.

3.2. Hysteresis current control

The dynamic behavior of the MRV is illustrated in the employment case of the ordering of the current by hysteresis.

The results shown in Fig. 8 were achieved from $\theta_{on} = 0°$, $\theta_{off} = 30°$, with reference current $I_{ref} = 8$ A and without torque load. Fig. 8a shows the influence of hysteresis current control on the shape of the current. One can also observe in Fig. 8b the influence of this hysteresis current control on the torque of the phase. The ripple of total torque has high amplitude for the values of $\theta_{on} = 0°$ and $\theta_{off} = 30°$ as shown in Fig. 8d, and by consequence of the oscillations speed, as shown in Fig. 8c.

For a better general view, the mean torque variance is plotted as a function of I_{ref} and θ_{off}. One notes that for different values of reference current, there is always a θ_{off} value that maximizes the mean (see fig. 9).

The mean couple is calculated by the expression:

$$\overline{C}_e = \frac{1}{T}\int C_e dt \tag{9}$$

4. Conclusions

This paper describes and discusses in detail the modeling and simulation of the SRM. An effective nonlinear model of SRM was developed using current and torque look-up tables generated from its calculated flux linkage and torque characteristics by a finite element method using FEMM software. Current and torque can be found from these 2-dimensional

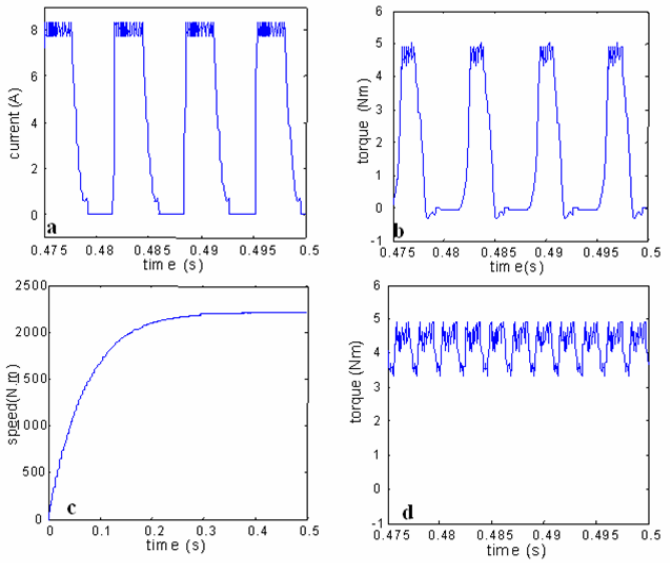

Figure 8: (a) Current in phase, (b) Torque in phase, (c) Speed and (d) Total torque

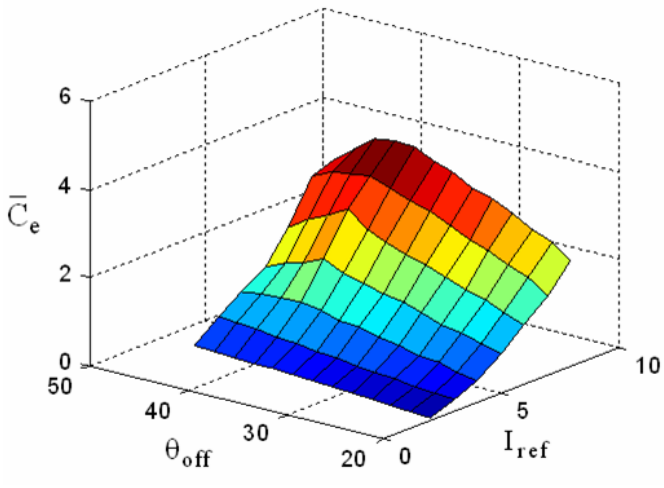

Figure 9: Mean torque as a function of I_{ref} and θ_{off}

look-up tables in a Matlab-Simulink environment. We verified that to analyze with precision the torque oscillation. Several simulations were performed to study the dynamic behavior of SRM; we mainly verified the influence of the turn-off angle θ_{off} on its dynamic behavior. It was proved to be dependent on the machine's operating point. A θ_{off} value was shown to exist which enables torque ripple reduction. For model validation, two strategies of order were simulated, phase current hysteresis and voltage control strategies. The results obtained are acceptable as a whole.

References

[1] C. Hao, P. Constantin, Large power analysis of switched reluctance machine system for coal mine, Mining Science and Technology 19 (2009) 657–659.

[2] H. M. Hasanien, S. M. Muyeen, J. Tamura, Torque ripple minimization of axial laminations switched reluctance motor provided with digital lead controller, Energy Conversion and Management 51 (2010) 2402–2406.

[3] H. Chen, V. Trifa, Design of 2000kw switched reluctance machine system, Procedia Earth and Planetary Science 1 (2009) 1380–1384.

[4] W. Ding, D. Liang, R. Tang, A fast nonlinear variable structure equivalent magnetic circuit modeling for dual-channel switched reluctance machine, Energy Conversion and Management 52 (2011) 308–320.

[5] M. Balaji, V. Kamaraj, Evolutionary computation based multi-objective pole shape optimization of switched reluctance machine, Electrical Power and Energy Systems 43 (2012) 63–69.

[6] Q. Song, X. Wang, L. Guo, L. Cheng, Double switched reluctance motors parallel drive based on dual89c52 single chip microprocessors, Procedia Earth and Planetary Science 1 (2009) 1435–1439.

[7] T. S. Chuang, Acoustic noise reduction of a 6/4 srm drive based on third harmonic real power cancellation and mutual coupling flux enhancement, Energy Conversion and Management 51 (2010) 546–552.

[8] S. Shoujun, L. Weiguo, D. Peitsch, U. Schaefer, Detailed design of a high speed switched reluctance starter/generator for more/all electric aircraft, Chinese Journal of Aeronautics 23 (2010) 216–226.

[9] S. Liu, G. Tan, G. Luo, X. Zhang, Z. Ma, Magnetic performance of shearer switched reluctance motors drive, Procedia Earth and Planetary Science 2 (2011) 98–103.

[10] H. A. Zarchi, G. R. A. Markadeh, J. Soltani, Direct torque and flux regulation of synchronous reluctance motor drives based on input-output feedback linearization, Energy Conversion and Management 51 (2010) 71–80.

[11] L. dos Reis, A. Coelho, O. Almeida, J. Campos, Modeling and controller performance assessment for a switched reluctance motor drive based on setpoint relay, ISA Transactions 48 (2009) 206–212.

[12] H. J. Chen, S. L. Lu, L. X. Shi, Development and validation of a general-purpose asic chip for the control of switched reluctance machines, Energy Conversion and Management 50 (2009) 592–599.

[13] S. C. Wang, An fully-automated measurement system for identifying magnetization characteristics of switched reluctance motors, Measurement 45 (2012) 1226–1238.